Chemistry–A European Journal
Research Article
doi.org/10.1002/chem.202401682
Chemistry Europe
European Chemical Societies Publishing
www.chemeurj.org

Tetrazole and Oxadiazole Derivatives as Thermally Activated Delayed Fluorescence Emitters

Céline Leonhardt[+],[a] Anna Mauri[+],[b] Idoia Garin[+],[c] Nils W. Rosemann,[c] Wolfgang Wenzel,[b] Uli Lemmer,[c] Mariana Kozlowska,*[b] and Stefan Bräse*[a, d]

Organic light-emitting diodes (OLEDs) are promising lighting solutions for sustainability and energy efficiency. Incorporating thermally activated delayed fluorescence (TADF) molecules enables OLEDs to achieve internal quantum efficiency (IQE), in principle, up to 100%; therefore, new classes of promising TADF emitters and modifications of existing ones are sought after. This study explores the TADF emission properties of six designed TADF emitters, examining their photophysical responses using experimental and theoretical methods. The design strategy involves creating six distinct types of a donor-acceptor (D–A) system, where tert-butylcarbazoles are used as donors, while the acceptor component incorporates three different functional groups: nitrile, tetrazole and oxadiazole, with varying electron-withdrawing character. Additionally, the donor-acceptor distance is adjusted using a phenylene spacer, and its influence on TADF functionality is examined. The clear dependency of an additional spacer, inhibiting TADF, could be revealed. Emitters with a direct donor-acceptor connection are demonstrated to exhibit TADF moderate emissive behavior. The analysis emphasizes the impact of charge transfer, singlet-triplet energy gaps (ΔE_{ST}), and other microscopic parameters on photophysical rates, permitting TADF. Among the emitters, **TCz-CN** shows optimal performance as a blue-green emitter with an 88% photoluminescence quantum yield (PLQY) and fast rate of reversible intersystem crossing of $2\times10^{6}\ s^{-1}$ and $1\times10^{7}\ s^{-1}$, obtained from time-resolved photoluminescence (TRPL) experiment in PMMA matrix and quantum mechanical calculations, respectively. This comprehensive exploration identifies molecular bases of superior TADF emitters and provides insights for future designs, advancing the optimization of TADF properties in OLEDs.

Introduction

Thermally activated delayed fluorescence (TADF) has emerged as a highly promising avenue in the realm of organic light-emitting diodes (OLEDs), showcasing its remarkable potential in enhancing device performance.[1–3] Unlike traditional fluorescent emitters, TADF emitters can achieve a theoretical internal quantum efficiency (IQE) of 100%, positioning them as promising contenders in the quest for improved OLEDs.[4,5,6] In addition, due to environmental concerns deriving from heavy metals, it is desirable to step away from phosphorescent emitters and seek solutions with purely organic compounds. The progress in TADF materials has been notably propelled by the development of exclusively organic emitters, outperforming phosphorescent emitters in OLEDs.[7] The introduction of novel TADF materials based on the carbazole/nitrile compound has underscored the potential of fully organic materials in TADF OLEDs.[8,9]

TADF mechanism in organic material enables, upon light absorption, the harvesting of both singlet and triplet excitons to achieve efficient light emission.[1,3–5] In particular, after the formation of the triplet exciton, the key process is the reverse intersystem crossing (RISC), which enables the reversion back to the singlet exciton.[1,3–5] After this process, energy is released in the form of delayed fluorescence, and since both singlet and triplet excitons contribute, TADF allows for the utilization of triplets that would otherwise be non-emissive or participate in other photophysical processes. Therefore, necessary conditions for TADF emitters are (i) small energy gap between the S_1 and T_1 state, ΔE_{ST} (< 0.2 eV), allowing for a molecule in a triplet state to go back to the singlet state,[5,10] (ii) small overlap of the highest occupied molecular orbital (HOMO) with the lowest unoccupied molecular orbital (LUMO)[1,2,5,11] and (iii) sufficiently high RISC rate, k_{RISC}, (typically above $10^{5}\ s^{-1}$).[2,5,10,12] The last parameter depends on ΔE_{ST} but requires adequate spin-orbit coupling between states and may be impacted by structural

[a] C. Leonhardt,[+] S. Bräse
Institute of Organic Chemistry, Karlsruhe Institute of Technology (KIT), Kaiserstraße 12, 76131 Karlsruhe, Germany
E-mail: stefan.braese@kit.edu
[b] A. Mauri,[+] W. Wenzel, M. Kozlowska
Institute of Nanotechnology, Karlsruhe Institute of Technology (KIT), Kaiserstraße 12, 76131 Karlsruhe, Germany
E-mail: mariana.kozlowska@kit.edu
[c] I. Garin,[+] N. W. Rosemann, U. Lemmer
Light Technology Institute, Karlsruhe Institute of Technology (KIT), Kaiserstraße 12, 76131 Karlsruhe, Germany
[d] S. Bräse
Institute of Biological and Chemical Systems – IBCS-FMS, Karlsruhe Institute of Technology (KIT), Kaiserstraße 12, 76131 Karlsruhe, Germany
E-mail: stefan.braese@kit.edu
[+] These authors contributed equally

Supporting information for this article is available on the WWW under https://doi.org/10.1002/chem.202401682Supporting information for this article is available on the WWW under https://doi.org/10.1002/chem.202401682

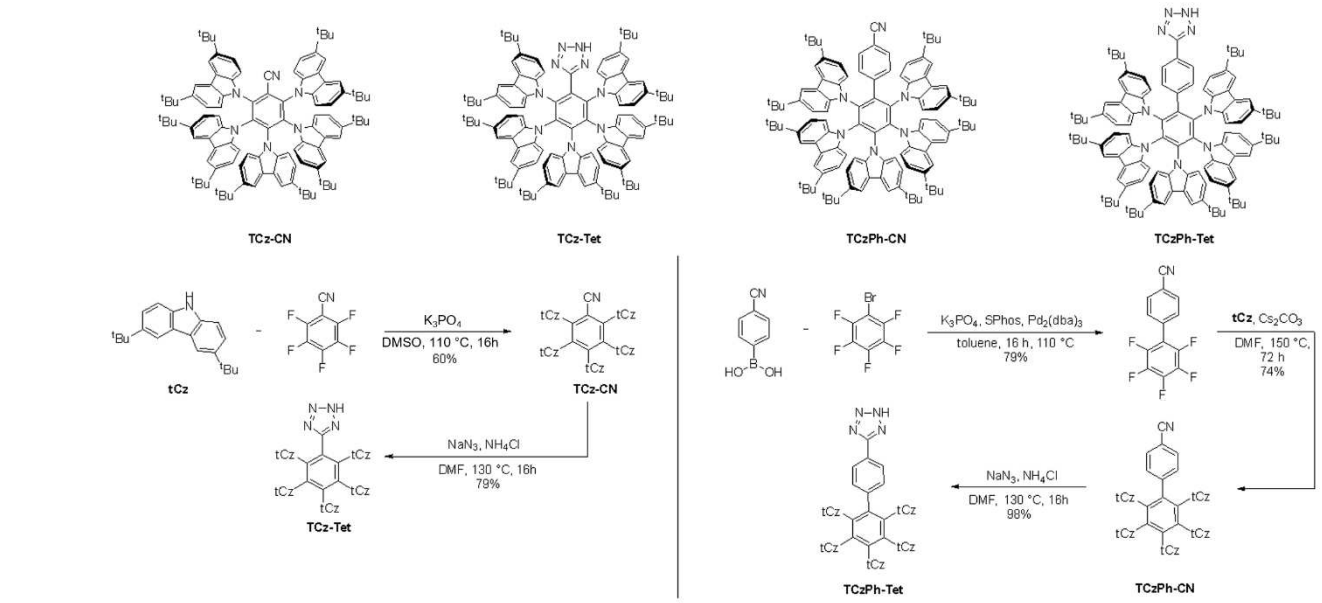

Scheme 1. Synthesis of potential benzonitrile and tetrazole TADF emitters with and without phenylene spacer.

confinement. These parameters can be fine-tuned through careful molecular design and customized according to specific requirements and preferences. Adhering to these principles, Adachi and colleagues in 2012 pioneered the development of efficient TADF emitters.[5] Notably, they have demonstrated that the carbazoloyl dicyanobenzene series achieves remarkable external quantum efficiencies (EQEs) of up to 19%. Among OLEDs showcasing the prowess of the green emitter, **4CzIPN**[5] was pointed out as the most efficient. A similar TADF system with up to five carbazole derivative donors attached to a nitrile acceptor was published by Zhang et al.[13] In contrast to Adachi's emitter series, Zhang's system employed benzonitrile instead of phthalonitrile and intriguingly, the omission of one nitrile acceptor unit in this configuration led to a TADF emission with a distinctly bluer hue. Moreover, the use of tertbutyl carbazole instead of carbazole as donors stabilized the TADF molecule through its bulky tertbutyl groups, which shielded the luminescent core, leading to a promoted photoluminescence efficiency and improved stability. In this way, OLED devices of Zhang et al.[13] with TADF molecules having the bulky tertbutyl groups achieved a higher EQE than those with the same molecular core with solely carbazole donors.

Leveraging the enhanced stability and efficiency offered by the 3,6-di-tert-butyl-9H-carbazole donor in the TADF emitters class, we sought to optimize the **5TCzBN** acceptor (depicted in Scheme 1, named here **TCz-CN**), to enhance the emissive properties of the investigated molecules. Prior research indicated that introducing an extra phenylene spacer between the donor and acceptor could push the emission spectrum further toward the blue, which is attributed to the weakening effect on the acceptor molecule.[14] Consequently, our strategic approach involved the initial modification of the nitrile acceptor of **5TCzBN**, transforming it into tetrazole and oxadiazole derivatives (**TCz-Tet**, **TCz-Me-Ox**, **TCz-ArF-Ox**, **TCz-AlkF-Ox**, Scheme 1 and Scheme 2) followed by the subsequent expansion of the molecular structure by incorporating an additional spacer (**TCzPh-CN** and **TCzPh-Tet**, Scheme 1), aiming to achieve a hypsochromic shift in the emission spectrum. Therefore, in this work, we aimed to investigate the TADF properties of a series of molecules, depicted in Scheme 1, for which the design of a twist-induced charge transfer (TICT)[1,15–17] donor-acceptor (DA) structure, known to be applied for constructing TADF emitters, was adopted. Such structural design should enhance the charge transfer phenomenon, permitting TADF.

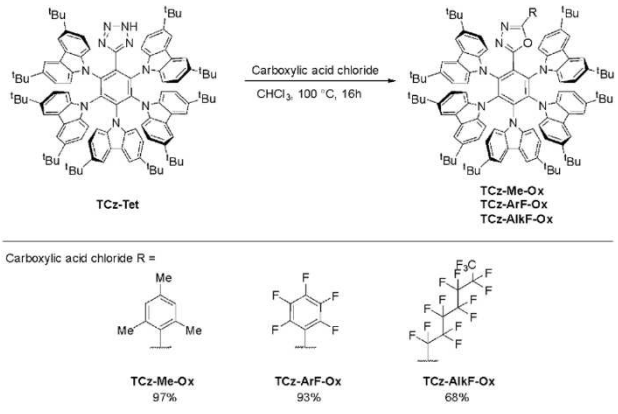

Scheme 2. Synthesis of oxadiazole TADF emitters **TCz-Me-Ox**, **TCz-ArF-Ox**, and **TCz-AlkF-Ox** using the corresponding carboxylic acid chloride.

Results and Discussion

The design of two main different types of TADF emitters was aimed. Firstly, a carbazole donor core with direct attachment of an acceptor was pursued (see Scheme 1). Secondly, a phenylene spacer was installed between the carbazole donor core and the acceptor, as depicted in Scheme 1. Nitrile, tetrazole, and oxadiazole groups were attached to the two core types. This resulted in six new molecules, further studied experimentally using photoluminescence to reveal their emissive properties and computationally to understand molecular bases of photophysical responses. The 2,3,4,5,6-penta(9H-carbazol-9-yl)benzonitrile (**TCz-CN** in this work), reported by Zhang et al.,[13] was used in our study for comparison.

The potential TADF emitters with a phenylene spacer between the acceptor and donor were synthesized as follows (Scheme 1). Nitrile **TCzPh-CN** was obtained within a two-step synthesis starting with the Suzuki cross-coupling reaction of 1-bromo-2,3,4,5,6-penta-fluorobenzene with (4-cyanophenyl)boronic acid under palladium catalysis to obtain 4-(2,3,4,5,6-pentafluorophenyl)benzonitrile in a 79% yield. Subsequently, 4-(2,3,4,5,6-pentafluorophenyl)benzonitrile was reacted with 3,6-di-tert-butyl-9*H*-carbazole (**tCz**) and cesium carbonate in an SN_{Ar} reaction to obtain **TCzPh-CN**. **TCzPh-Tet** was obtained by reacting **TCzPh-CN** and sodium azide in a 1,3-dipolar cycloaddition, yielding TCzPh-Tet with 98% yield.

The other TADF emitters, without a spacer, were obtained starting with 2′,3′,4′,5′,6′-pentafluoro-4-carbonitrile, **tCz**, and tripotassium phosphate resulting in **TCz-CN** with a yield of 60%. To gain the corresponding tetrazole, **TCz-Tet**, **TCz-CN**, and sodium azide were used, giving a 79% yield.

Later, another acceptor was established from the photophysical experiments, which will be discussed in the next section. **TCz-Tet** was transformed into oxadiazoles via the Huisgen reaction with three carboxylic acid chlorides[18] (Scheme 2). The residues of the carboxylic acid chlorides have been chosen depending on the desired electronic properties of the final TADF emitters: either more electron-withdrawing, fluorine, or electron-donating methyl groups. 2,4,6-Trimethylbenzoyl chloride was added to **TCz-Tet**, delivering a relatively weak acceptor, **TCz-Me-Ox** (97%). In contrast, two stronger acceptor residues have been added with pentafluorobenzoic acid chloride, giving **TCz-ArF-Ox** (93% yield) and pentadecafluorooctanoyl chloride, giving **TCz-AlkF-Ox** (68%). All six potential TADF emitters have been fully characterized using nuclear magnetic resonance spectroscopy (NMR), mass analytic spectrometry (MS), and infrared spectroscopy (IR), which confirmed the successful synthesis of all six molecules. The results of all analyses mentioned are listed in the Supporting Information (SI). Furthermore, all compounds were analyzed via photophysical measurements, and complementary quantum mechanical calculations were performed.

Photophysical Characterization

The photophysical properties of the emitters were evaluated spectroscopically first in a dilute toluene solution (see Table 1 and Figure S9). Later, the steady-state photoluminescence (PL) of dopped films with PMMA (polymethyl methacrylate) as a matrix and emitters in 5%wt was measured (data depicted in Figure 1). All the compounds show similar absorption spectra: In Figure S9, two intense absorption peaks are visible, i.e., at approximately 350 nm and 300 nm. The peak at 350 nm is highly broadened. A similar observation was derived by theoretically calculated spectra in the gas phase and implicit toluene depicted in Figure S16 and S17. They show that **TCz-CN**, **TCz-ArF-Ox**, and **TCz-AlkF-Ox** exhibit maximum absorption at 323 nm, 321 nm, and 322 nm with an oscillator strength of 0.26, 0.28, and 0.31, respectively, while **TCzPh-CN**, **TCzPh-Tet**, **TCz-Tet**, and **TCz-Me-Ox** show maximum at approximately 318 nm, 319 nm, 314 nm, and 317 nm with an oscillator strength of 0.28, 0.35, 0.45 and 0.27, respectively (Figure S16). The absorption related to the S0→S1 transition peaked at 374 nm, 343 nm, 373 nm, and 374 nm with oscillator strength of 0.21, 0.19, 0.15 and 0.19 for **TCz-CN**, **TCz-Me-Ox**, **TCz-ArF-Ox**, and **TCz-AlkF-Ox**, while **TCz-Tet**, **TCzPh-Tet** and **TCZPh-CN** show absorption at 338 nm, 354 nm and 340 nm with oscillator strength of 0.18, 0.12 and 0.13. The orbital contribution of these transitions for all compounds is listed in Table S4.

The PL emission maxima of the solutions range from deep blue (439 nm) to green (522 nm), see Figure S9 and Table 1. The predecessor emitters, i.e., **TCzPh-CN** and **TCzPh-Tet**, have deep blue emissions with the maximum peak position at $\lambda = 450$ nm and $\lambda = 439$ nm, respectively. The derivative emitters have red-shifted emission: to sky-blue, i.e., e.g., **TCz-CN** ($\lambda = 475$ nm), and to green, i.e., **TCz-ArF-Ox** ($\lambda = 506$ nm), and (**TCz-AlkF-Ox** $\lambda =$ 522 nm). The emission in all cases is relatively narrow, with full-

Table 1. Steady state and time-resolved PL data for compounds in toluene solutions.

Compound	λ_{Max} (nm)	FWHM (cm^{-1})	τ_{PF} (ns)	τ_{DF} (μs)	Φ_{DF}/Φ_{PF}
TCzPh-CN	450	3412	2.64	–	–
TCzPh-Tet	439	3496	3.02	–	–
TCz-CN	475	3571	4.40	9.8	4.98
TCz-Tet	450	6064	3.81	1.7	0.60
TCz–Me-Ox	441	4326	1.96	10.9	2.44
TCz-ArF-Ox	506	3984	4.70	1.2	5.19
TCz-AlkF-Ox	522	4044	7.21	1.90	8.58

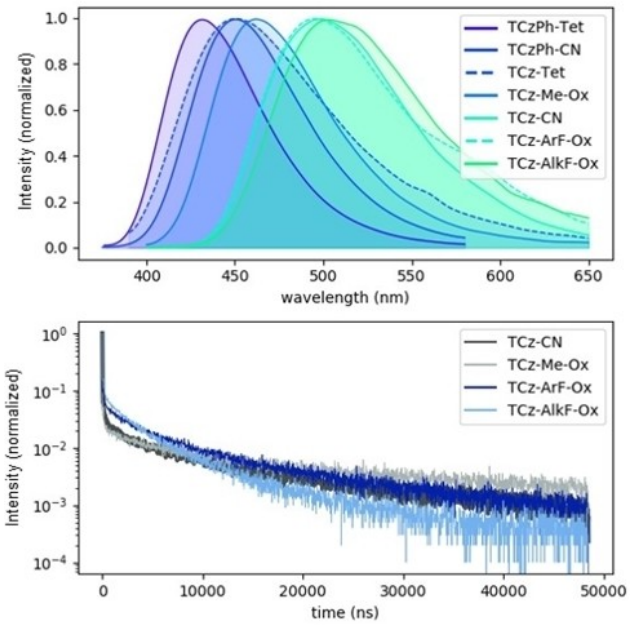

Figure 1. Steady-state PL spectra (top) and TRPL emission (bottom) of the emitters in 5 %wt PMMA films with 370 nm excitation.

width half maximum (FWHM) values ranging from 3412 cm^{-1} to 6064 cm^{-1}. **TCzPh-CN** shows the narrowest FWHM, while **TCz-Tet** has the widest FWHM. No significant overlap exists between the absorption and emission spectra (see Figure S9), indicating a low degree of reabsorption present.

The time-resolved PL measurements of the degassed solutions show nanoseconds-long monoexponentially decays for the predecessor molecules **TCzPh-CN**, **TCzPh-Tet**, while the derivative molecules **TCz-CN**, **TCz-Me-Ox**, **TCz-ArF-Ox**, and **TCz-AlkF-Ox** decay biexponentially with a large delayed component, as can be seen in Figure S10. The derivative molecule **TCz-Tet** only has a negligible delayed component. As is typical in TADF molecules, the prompt components are in the order of nanoseconds, and the delayed components last for microseconds (see Figure S10). The prompt components show lifetimes between 2 ns and 7 ns. The delayed components have been found in the emitters with biexponential decay, ranging from 1 μs to 11 μs.

The emitters' photophysical behavior was then tested in spin-coated PMMA thin films with a 5 wt% emitter concentration. The results are summarized in Table 2. Figure 1 shows the PL of the films. The emission in the doped-PMMA films indicates a slight blue shift of bands compared to the toluene solutions, i.e., to 432 nm, 450 nm, and 503 nm in films. There is also a general widening of the emission resulting in FWHM from 3557 cm^{-1} to 4875 cm^{-1}, which was also observed for emitters in toluene. The films' photoluminescence quantum yield (PLQY/ Φ_{PL}) was measured in air and an N_2 environment with 365 nm excitation. **TCz-CN** has the highest PLQY - 87.8% in N_2 and 65.6% in air. All the compounds show a significant decrease (~20%) in PLQY values from N_2 to air; therefore, this is an indication that triplets are probably involved in the luminescence mechanism. All of the derived molecules have higher PLQY values than the predecessor molecules **TCzPh-CN** and **TCzPh-Tet** except for **TCz-Tet**, whose 40% is the lowest PLQY in N_2 of all compounds (45–88% PLQY is found for other molecules). Despite the clear influence of O_2 in the compounds' PLQY values, not all display delayed emission components in the TRPL measurements. All emitters that showed TADF emission in solution behave similarly in the films.

The emitters with delayed emission show lifetimes τDF of several microseconds, as expected for TADF emitters. **TCz-CN** has a delayed emission lifetime of 5 μs, while TCz–Me-Ox, TCz-ArF–Ox, and **TCz-AlkF-Ox** have 8 μs, 2.5 μs and 2.5 μs, respectively. All emitters have nanosecond-short prompt emission lifetimes. The remaining compounds showed only prompt components in their emission (see Figure S11): the delayed component was too small to accurately measure by the technique applied, described in the Experimental Section.

As mentioned, we used the TRPL parameters and quantum yield measurements to quantify the processes involved in the decay following optical excitation; the results are listed in Table 2. Out of seven molecules studied, the four compounds (**TCz-CN**, **TCz-Me- Ox**, **TCz-ArF-Ox** and **TCz-AlkF-Ox**) are TADF active with similar photophysical rates: rate of fluorescence

Table 2. Photophysical results and kinetics of the emitters in 5 wt%-doped PMMA films. Maximum wavelength (λ_{max}), full width at half maximum (FWHM), and quantum yield (Φ_{PLQY}) of the emission spectrum. Decay-time of the prompt (τ_{PF}) and delayed (τ_{DF}) fluorescence as well as the ratio delayed-fluorescence intensity to prompt-fluorescence intensity (Φ_{DF}/Φ_{PF}). Rate of fluorescence (k_F), rate of intersystem crossing (k_{ISC}), rate of reverse intersystem crossing (k_{RISC}), nonradiative decay-rate from the triplet state (k_{nrT}), and energy gap between singlet- and triplet-state (ΔE_{ST}).

Compound	λ_{max} (nm)	FWHM (cm $^{-1}$)	τ_{PF} (ns)	τ_{DF}(μs)	Φ_{DF}/Φ_{PF}	Φ_{PLQY} (%)	k_F (10^7 s^{-1})	k_{ISC} (10^8 s^{-1})	k_{RISC} (10^6 s^{-1})	k_{nrT} (10^4 s^{-1})	ΔE_{ST} (meV)
TCzPh-CN	449	3695	2.97	–	–	65	–	–	–	–	–
TCzPh-Tet	432	3557	3.16	–	–	45	–	–	–	–	–
TCz-CN	496	3897	4.33	5	11.6	88	1.61	2.13	2.47	2.39	88.3
TCz-Tet	451	4875	3.91	–	–	40	–	–	–	–	–
TCz–Me-Ox	460	3664	2.64	8	19.5	72	1.31	3.60	2.53	3.59	57.0
TCz-ArF-Ox	494	4055	3.38	2.5	16.3	79	1.15	2.98	5.97	5.85	102.6
TCz-AlkF-Ox	503	3788	3.40	3.6	21.0	78	0.91	2.82	8.50	12.2	86.5

k_F~10^7 s^{-1}, the rate of intersystem crossing (ISC) k_{ISC}~10^8 s^{-1}, rate for reverse intersystem crossing k_{RISC} 10^6 s^{-1} and rate of triplet nonradiative decay k_{nrT}~10^4 s^{-1}. The k_{RISC} values of ~up to $8.5{\cdot}10^6$ s^{-1} are comparable to previous reports, where k_{RISC} values above 10^7 have been achieved.[19]

The contribution of the delayed components to the observed emission is up to 21 times higher than that of the prompt emission (c.f. the Φ_{DF}/Φ_{PF} ratios), which is in line with the observed high rates of k_{RISC}. When comparing between the emitters, the factor that appears to be a better predictor of a high PLQY value is a low k_{nr}. Despite **TCz-CN** having the lowest k_F and k_{RISC} of the four TADF emitters, it possesses the group's highest PLQY and lowest k_{nr}.

Finally, the temperature dependence of the films' emission was measured, as shown in Figure 2. The decrease of the delayed component with a decrease in the temperature confirms the presence of TADF. To determine the ΔE_{ST} of the molecules through Arrhenius plots (see Figure S13), k_{RISC} values were calculated at each temperature and are depicted in Figure 2. The ΔE_{ST} values were between 57 and 103 meV, following other emitter molecules of similar structure; e.g., **4CzIPN** has a ΔE_{ST} of 87 meV.[5] For the higher-performance blue TADF emitters, ΔE_{ST} as low as 13.4 meV has been found.[20]

DFT Calculations

To further explain the TADF activity of the molecules studied, quantum mechanical calculations based on the density functional theory (DFT) and time-dependent DFT (TD-DFT) have been performed. Specifically, we were interested in the elucidation of the reasons behind the lack of TADF activity in **TCzPh-CN**, **TCzPh-Tet**, and **TCz-Tet**, as observed in experiments, and the explanation of favorable TADF emissive performances for **TCz-CN**, **TCz-ArF-Ox**, **TCz-AlkF-Ox**, and **TCz-Me-Ox**. Firstly, the HOMO-LUMO gap, representing the energy difference between the frontier orbitals ($\triangle E{=}E_{LUMO}{-}E_{HOMO}$) as either a fundamental or an optical gap,[21] was calculated. The latter considers the energy of LUMO orbitals to explicitly account for fluctuations in the electron density upon singlet excitation. The results are listed in Table S4, while the molecular orbitals (MO) are depicted in Figure 3. As expected, the HOMO and LUMO orbitals are well separated with the formers being mostly localized on the electron-rich carbazole-donor unit, while the

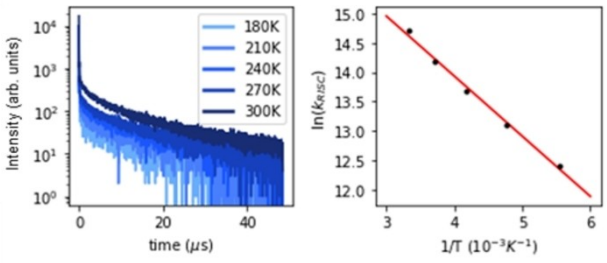

Figure 2. Temperature-dependent TRPL measurements (left) and Arrhenius plot (right) of PMMA:**TCz-CN** films (5%wt).

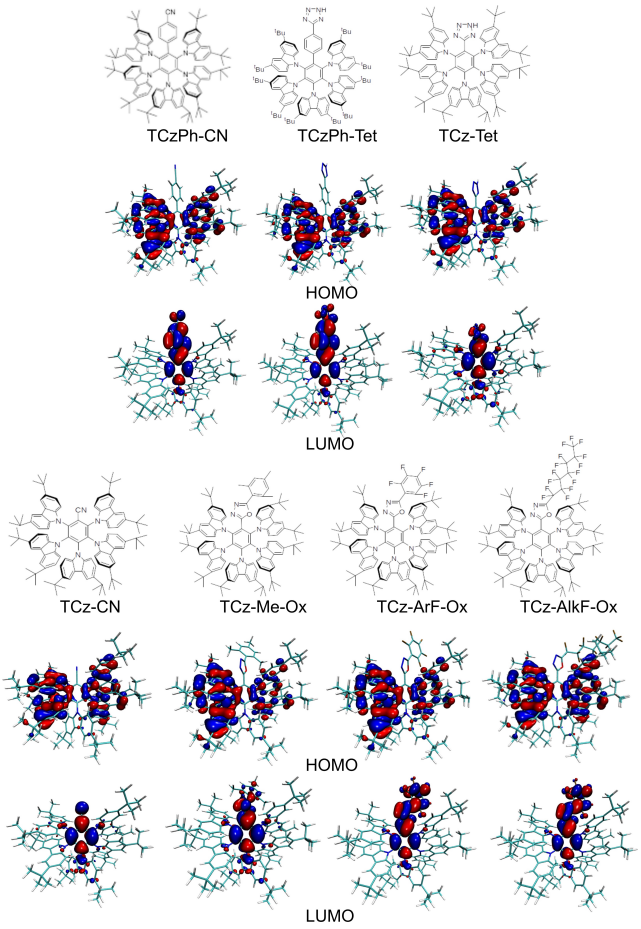

Figure 3. Chemical structures and frontier orbitals of **TCzPh-CN**, **TCzPh-Tet**, **TCz-CN**, **TCz-Tet**, **TCz-Me-Ox**, **TCz-ArF-Ox**, and **TCz-AlkF-Ox**. The visualization of HOMO and LUMO orbitals was performed employing Visual Molecular Dynamics (VMD), version 3.6, based on data obtained using TDA-BMK–D3(BJ)/def2-SVP level of theory. An isovalue of 0.002 a.u. was used for visualization. The respective energies of orbitals are listed in Table S4.

electron density in the letters occupies the respective acceptor unit, an important sign of the TADF activity. The strategic design of electron donor and acceptor components for typical TADF emitters holds significant importance, requiring the balance between the HOMO-LUMO overlap and S_1–T_1 energy gap ($\triangle E_{ST}$).[1,5,10,22] The orbital overlap, important for the final quantum yield, is visualized in Figure 4 and it is discussed in more details further. The HOMO→LUMO transition upon the lowest singlet excitation consistently dominates across all investigated systems (e.g., exceeding 80%, Table S4) where TADF active molecules show higher HOMO→LUMO contribution (in most cases, it is higher than 90%) than molecules characterized by the lack of TADF. From experimental measurements presented in Figure 1 and the calculated absorption characteristics of molecules in Figure S16 and S17, we have also noticed that the HOMO-LUMO optical gap for inactive TADF emitters (**TCzPh-CN**, **TCzPh-Tet**, and **TCz-Tet**) is generally greater (i.e., 3.51 eV, 3.64 eV, and 3.67 eV, see Table S4) compared to TADF-active molecules (consistently 3.32 eV), except **TCz-Me-Ox**, which exhibits a slightly larger gap (3.55 eV). However, according to the experimental measurements, it belongs to the

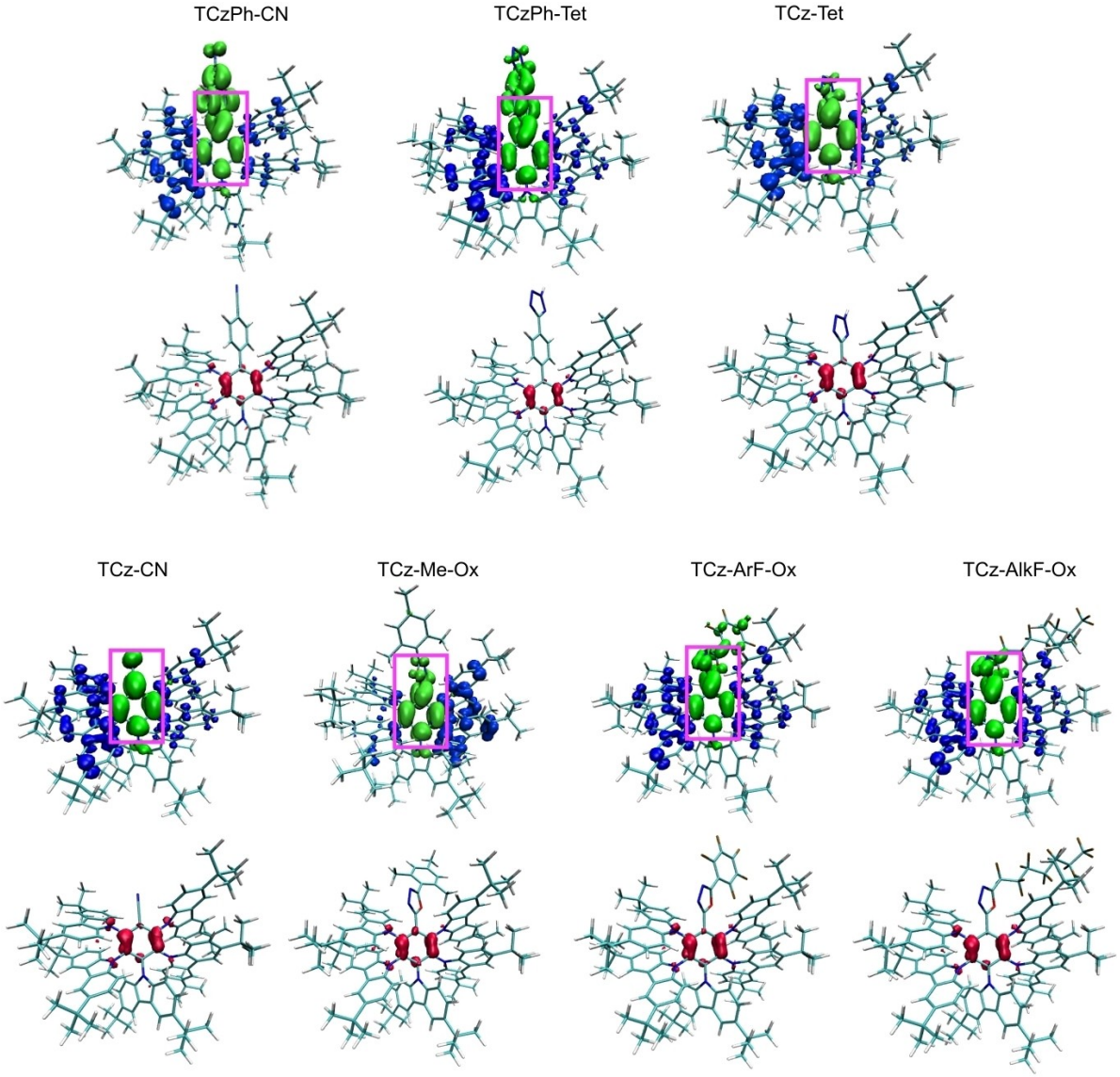

Figure 4. Visualization of electron-donating (hole, in blue) and electron-accepting (electron, in green) regions involved in the electron density transfer during first singlet excitation. The respective overlap (in red) of hole and electron densities upon excitation from the ground state to the first singlet state (S_1) in the gas phase. The area where electrons are localized in the measured TADF active molecules is depicted in pink. An isovalue of 0.002 a.u. was used for visualization. The excitation to the first triplet state is depicted in Figure S14.

TADF emitter class. The cause of its similarities to TADF inactive emitters in terms of the HOMO-LUMO gap is probably connected to the impact of other processes on the reactivity of the molecule, e.g., charge transfer (CT) characteristics, spin-orbit coupling (SOC), reorganization energy, which are discussed further. Therefore, the distance, separating the HOMO and LUMO, is a determining factor for which emitters displayed delayed emission. In the case of **TCzPh-CN** and **TCzPh-Tet**, the spacer unit between the donor and the acceptor might be responsible for this separation.

The subsequent analysis focused on the electron density difference between the electron-donating (hole) and electron-accepting (electron) components that follow excitation from the ground state to the first singlet state. The resulting disparities in electron density upon excitation are depicted in Figure 4. Additionally, the CT parameters[28] characterizing the transition from the optimized ground state to the lowest excited singlet state (S_1) during both the absorption and the subsequent relaxation of the S_1 geometry for all investigated systems are reported in Table S5. The data obtained reveal that the CT in TADF inactive emitters, such as **TCzPh-CN** and **TCzPh-Tet**, is notably distance prolonged compared to the other investigated molecules, involving the entire acceptor: the CT distance varies from around 1.23–2.02 Å for TADF active molecules (**TCz-CN**, **TCz-Me-Ox**, **TCz-ArF-Ox**, and **TCz-AlkF-Ox**), up to 2.71–2.87 Å for **TCzPh-CN** and **TCzPh-Tet**. All transitions exhibit relatively large values (i.e., >2.54 Å) of the average degree of the spatial extension of electrons and holes distribution (H_{CT}), with the highest (excluding **TCz-ArF-Ox**) values for inactive **TCzPh-CN** and **TCzPh-Tet**, indicating wide

hole and electron distribution of these transitions. H_{CT} values of other compounds are slightly lower, indicating that the hole and electron distribution for these TADF emitters are narrower than for the formers. This phenomenon is attributed to the increased separation between the donor and acceptor in the formers facilitated by the additional phenyl spacer. The exception is **TCz-ArF-Ox**, for which it is evident that the distribution of electrons (mostly) covers the entire acceptor group, leading to a higher H_{CT} value of 2.95 Å. The CT properties of **TCz-Tet** cannot be directly connected to its TADF inactivity, which is explained below.

The overlap of holes and electrons for TADF emitters is slightly diminished, e.g., 0.32 au and 0.33 au in comparison to 0.32–0.37 au for the TADF active emitters (see regions in red in Figure 4 and Sr parameter in Table S5). High values for the total magnitude of charge transfer length (listed in Table S5) combined with higher HOMO-LUMO gap provide further confirmation for this observation. Consequently, we can assert that charge transfer is predominantly influenced by the length of the acceptor, which, in the case of **TCzPh-CN** and **TCzPh-Tet**, is significantly extended. In addition, while the differences in the hole delocalization indices (HDI) between TADF emitters and non-emitters are quite small, the electron delocalization indices (EDI) of inactive TADF emitters, as **TCzPh-CN** and **TCzPh-Tet**, differ more: this is connected to the fact that the electrons of **TCzPh-CN** and **TCzPh-Tet** have a higher degree of delocalization on the acceptor part. Also, **TCz-ArF-Ox** is characterized by a smaller EDI index concerning the active TADF emitters, as can be seen by the fact that the electrons are more delocalized on the acceptor part involving the pentafluorophenyl, contrary to what happens in **TCz-Me-Ox**, where the phenyl ring is not involved in the CT.

As previously reported,[1], charge transfer is crucial for reducing the HOMO-LUMO gap, leading to a closer singlet-triplet gap.[1,5,23] However, in the case of **TCzPh-CN** and **TCzPh-Tet**, the exceptionally high HOMO-LUMO gap and the substantial charge transfer from donor to acceptor may suppress TADF emission and do not favor the fluorescence emission properties.[24] This indicates that TADF materials' efficacy is intricately linked to a delicate balance in molecular properties, and a certain degree of overlap between hole and electron is necessary for enhancing TADF emission without suppressing the emission.

The dihedral angle (θ) between donor and acceptor moieties is also a key factor in controlling the charge transfer feature:[1] the TADF emitters with θ close to 90° were previously designed to largely separate the HOMO and LUMO, almost vanishing the S–T energy gap.[15,16] In Table S6 and Figure S15, the θ angle between the donor and acceptor parts of the molecules investigated is reported: values are 30–37° for the S_1 state, 30–51° for the T_1 state of all molecules. The TADF inactive emitters are characterized by slightly larger values of the θ angle (approximately 38° in the S_1 state), in agreement with the larger CT shown (see Figure 4 and Table S5). The data obtained are in line with the previously reported S–T energy gaps of 0.31 eV and 0.11 eV for values of dihedral angles of 48° and 87°, respectively.[15]

Although the results presented do not reveal any notable distinction for the TADF inactive molecule **TCz-Tet** compared to the TADF emitters, it becomes apparent, upon examining the chemical structure of this molecule, that the presence of the tetrazole acceptor unit might account for its TADF inactivity due to molecular instability. Indeed, if the molecular design is not optimized, acceptors containing tetrazole could potentially extinguish the TADF effect by, for instance, the ring opening phenomenon, which increases the molecular instability and leads to a quench of the TADF effect. This was demonstrated by Guerra et al.[25] who found that the photochemical generation of nitrile imine compounds from tetrazoles involves a complex mechanism with distinct electronic rearrangements and bond-breaking processes. Observing the evolution of the electronic structure connecting relevant energy stationary points, the study revealed that the N–N bond breaks once the S_1-excited tetrazole reaches the higher triplet state (T_2), leading to a radical cation intermediate. Subsequently, at the T_2/T_1 crossing, the C–N bond homolytically breaks, resulting in the full ring opening phenomenon.

In the case of **TCz-Tet**, although the PLQY measurements of the films under 365 nm excitation in both air and N_2 environments are 23% and 40%, respectively, indicating the presence of triplet states, no TADF is observed because deactivation via bond breaking occurs in the tetrazole moiety.[25]

To address the singlet-triplet energy gap of molecules studied, the vertical excitation energies for all systems studied have been calculated (listed in Tables S7 and S8). For all TADF active molecules, the S–T gap is close to 0.20 eV (0.21–0.23 eV for **TCz-ArF-Ox**, **TCz-AlkF-Ox**, and **TCz-CN**, respectively), with a slightly higher value for **TCz-Me-Ox** (0.34 eV). At the same time, the spin-orbit coupling between excited states of **TCz-Me-Ox** is in the range of TADF active molecules (see Table S10), which probably allows delayed emission. All TADF inactive molecules have higher ΔE_{ST}, i.e., 0.30–0.40 eV and therefore, designed molecules demonstrate TADF consistent with commonly known trends. We should note that all values of ΔE_{ST} calculated are slightly higher than energy differences obtained experimentally (see Table 2), characteristic of the TD-DFT method.[27] Therefore, the GW-BSE approach (one-body Green's function approximation with dynamically screened Coulomb interaction and Bethe-Salpeter equation) has also been utilized (see Table S9). However, this approach failed to reproduce trends of the energy difference, systematically overestimating energy gaps, making it unsuitable for the molecules studied in this paper. Complementary to experiments, we have calculated rates of radiative (fluorescence, k_F) and nonradiative (internal conversion (k_{nrS}) and (reverse) intersystem crossing ($k_{(R)ISC}$) using k_{nrTS} for the ISC T_1-S_0) decay using methodology explained in detail in the Supporting Information. All data is listed in Table 3; overall, the computed values correlate well with the experiment.

Fluorescence rates are approximately in the order of ~10^7 s^{-1}, consistent with the experimentally reported values (Table 2). They are competitive with k_{nrS} while the slightly higher k_{nrS} compared to k_F for some of the molecules is caused by considering the calculations in the gas phase without the impact of the PMMA matrix. The k_{ISC} rates, computed consider-

Table 3. Computed $S_0 \rightarrow S_1$ absorption (λ_{abs}) and fluorescence (λ_F), rate of internal conversion $S_1 \rightarrow S_0$ (k_{nrSS}), fluorescence (k_F), intersystem crossing (k_{ISC}), reverse ISC (k_{RISC}) and nonradiative decay of the triplet state (k_{nrTS}) for all molecular systems studied in the gas phase calculated with TDA-BMK–D3(BJ)/def2-SVP level of theory. All rates are in s^{-1} and were computed using the approach described in Theoretical calculations and section 5 in SI. k_{ISC} and k_{RISC} were calculated using reorganization energy from optimized triplet state to optimized singlet state (see λ T–S), and both the adiabatic (including zero-point energy correction (ZPVE), ΔE, see Table S11) and vertical energy gap (ΔE_{vert}) between singlets and triplets ($k_{ISC/RISC}$ and $k_{ISCvert/RISCvert}$, respectively). The data for **TCzPh-CN** are unavailable due to computational constraints in the MOMAP software, while data for **TCz-ArF-Ox** are unavailable due to the absence of convergence of the correlation function in MOMAP. Inactive TADF emitters are marked in gray.

Compound	λ_{abs}	λ_F	k_{nrSS}	k_F	k_{ISC}	$k_{ISCvert}$	k_{RISC}	$k_{RISCvert}$	k_{nrTS}	ΔE	ΔE_{vert}	λT_1-S_1
TCzPh-CN	353	430	NA	NA	1.01×10^8	2.42×10^8	4.77×10^7	3.30×10^6	NA	0.32	0.30	0.30
TCzPh-Tet	340	402	1.55×10^7	1.07×10^7	1.27×10^7	5.15×10^7	1.81×10^4	3.55×10^3	8.36×10^2	0.23	0.40	0.77
TCz-CN	374	442	3.35×10^8	3.26×10^7	1.12×10^8	1.21×10^8	6.20×10^5	4.04×10^6	1.27×10^4	0.31	0.23	0.24
TCz-Tet	338	413	9.88×10^6	8.22×10^6	1.71×10^7	8.74×10^7	6.32×10^3	2.40×10^3	7.77×10^2	0.19	0.39	0.87
TCz-Me-Ox	349	431	1.39×10^8	3.21×10^7	3.29×10^8	3.83×10^8	4.18×10^5	5.70×10^5	7.66×10^4	0.38	0.34	0.19
TCz-ArF-Ox	373	479	NA	NA	NA	NA	NA	NA	NA	0.03	0.21	0.69
TCz-AlkF-Ox	374	490	1.98×10^8	1.76×10^7	1.35×10^7	1.21×10^7	6.69×10^7	8.98×10^6	1.60×10^4	0.22	0.21	0.30

ing the adiabatic S–T energy gap, are competitive with k_F and increase in the order **TCzPh-Tet**, **TCz-AlkF-Ox**, **TCz-Tet**, **TCzPh-CN**, **TCz-CN** and **TCz-Me-Ox**. In addition, the k_{ISC} rates calculated considering the vertical S–T energy gap show a similar trend. Finally, the k_{RISC} values computed with both adiabatic and vertical S–T energy gaps for TADF active molecules are in the range of 10^5–10^7 s^{-1}, while for the TADF inactive emitters, the values drop down to 10^3–10^4 s^{-1}, except for **TCzPh-CN**, which shows k_{RISC} value in the order of TADF active emitters. This is probably due to the smaller reorganization energy (i.e., 0.30 eV) and higher SOC (1.13 cm^{-1}, Table S10). It should be noted that reorganization energy, which is necessary to move the molecule from its structure in the lowest triplet to the structure in the lowest singlet state, was calculated here in the gas phase, and it may be smaller in the PMMA matrix since the structural moves of molecules may be more constrained. TADF active molecules considered possess reorganization energy in the range of 0.19–0.30 eV, while for TADF inactive systems, except for **TCzPh-CN**, it is larger than 0.77 eV (see Table 3), indicating that not only ΔE_{ST} indicates TADF functionality of new reported molecules. Moreover, it is noteworthy that the SOC values for TADF emitters are in the order of ~1 cm^{-1} (see Table S10), whereas for inactive TADF systems (except **TCzPh-CN**), they are approximately 0.20 cm^{-1}. The RISC rates for both TADF active and inactive compounds are faster than the nonradiative decay of the first triplet state (k_{nrTS}).

Conclusions

In conclusion, using the molecular strategy based on the implementation of a carbazole donor core with nitrile, tetrazoles and oxadiazole as acceptors, six molecules have been synthesized, starting from nitriles **TCz-CN** (used as reference from Zhang et al.[13]) and **TCzPh-CN**, tetrazoles **TCz-Tet** and **TCzPh-Tet** and via 1,3 dipolar cycloaddition. The tetrazole ring was modified into an oxadiazole following the Huisgen protocol. Optical spectroscopic measurements were applied to reveal synthesized molecules' different photophysical properties and emission characteristics. All compounds demonstrated PLQY efficiencies above 40%, with emission spectra ranging from deep blue to green. Time-resolved photoluminescence confirmed the presence of prominent TADF emission (up to 21 Φ_{DF}/Φ_{PF}) in four of the derivative compounds (**TCz-CN**, **TCz-Me-Ox**, **TCz-ArF-Ox**, and **TCz-AlkF-Ox**) in toluene solution and PMMA films while the remaining derivative emitter only displayed scarce TADF emission in solution. In addition, from the temperature-dependent measurements of the doped-PMMA films, we have found ΔE_{ST} values below 100 meV for the TADF emitters studied, demonstrating efficient TADF emission. This phenomenon has been further inspected using quantum mechanical calculations, showing similar photophysical rate dependencies for the investigated molecules.

From the experimental measurements, **TCz-CN** is the most efficient emitter (88%) despite not having the largest proportion of TADF or the highest k_{RISC}. To note that the k_F, τ_{DF} and Φ_{PLQY} values reported for this TADF emitter (1.61×10^7 s^{-1}, 5 μs and 0.88 reported in Table 2) are in agreement to previously reported data[13] of 0.87×10^7 s^{-1}, 3.4 μs and 0.13/0.86, respectively. From quantum mechanical calculations, we have noticed that **TCz-CN** meets all relevant criteria known for TADF molecules, i.e., its vertical ΔE_{ST} is 0.23 eV, SOC of 0.84 cm^{-1} (in the range of other TADF active molecules studied), reorganization energy is 0.24 eV, giving the k_{RISC} of 4.04×10^6 s^{-1}. Results computed in this work are also in agreement to data reported in Ref.,[13] with the HOMO-LUMO gap of 3.32 eV, vertical ΔE_{ST} of 0.23 eV, and optimized T_1 energy of 2.77 eV. Moreover, its k_{ISC} is ~1×10^8 s^{-1} (i.e., in the range of k_F and k_{nrS}), enabling triplet formation. Detailed analysis of the CT effects, overlap of frontier orbitals, and electron density difference performed on the new molecules studied in this work allowed us to classify them between active and inactive TADF emitters, as shown by the experimental photophysical measurements. New TADF active molecules reported here show similar properties to **TCz-CN**, exhibiting CT character upon excitation to the S_1 state. In addition, they show ΔE_{ST} in the range of 0.21-0.34 eV, competitive nonradiative and radiative rates, which are 10^5–10^8 s^{-1}, combined with SOC in the range of 0.90–1.07 cm^{-1}. Inactive

TADF emitters, such as **TCzPh-CN** and **TCzPh-Tet**, are characterized by a prominent CT due to the additional phenyl spacer, which is, indeed, responsible for the quenching of their TADF emission due to the lack of the balance between the CT and HOMO-LUMO overlap. For **TCzPh-Tet** and **TCz-Tet**, the unstable tetrazole group also plays an important role in reducing the TADF activity, most probably due to the bond breaking in the triplet states. Moreover, the k_{RISC} of these molecules is in the order of ~10^3–10^4 s^{-1}, competitive with the nonradiative decay of the triplet state of ~10^2 s^{-1}, but still lower than the ones for TADF active emitters (except for **TCzPh-CN**).

Experimental Section

The syntheses of the nitrile precursors 4-(2,3,4,5,6-pentafluorophenyl)benzonitrile, **TCz-CN** and **TCzPh-CN** are stated in the Supporting Information.

General Procedure for the Synthesis of Tetrazole Compounds TCz-Tet and TCzPh-Tet

A sealable vial was charged with nitrile **TCz-CN** or **TCzPh-CN** (1.00 equiv.), sodium azide (3.00 equiv.), and ammonium chloride (3.00 equiv.). Dry dimethylformamide (10 and 5 mL, respectively) was added, and the resulting mixture was heated at 130 °C for 16 h until completion. After cooling to room temperature, the reaction mixture was poured into an excess of 1 M hydrochloric acid (50 mL) and mixed thoroughly. The solid was filtered off, washed several times with water, and thoroughly dried to afford tetrazole compounds **TCz-Tet and TCzPh-Tet**.

General Procedure for the Synthesis of Oxadiazole Compounds TCz-Me-Ox, TCz-ArF-Ox and TCz-AlkF-Ox

A sealable vial was charged with tetrazole **TCz-Tet** (1.00 equiv.) and the corresponding acid chloride (4.00 equiv.). Chloroform (10 mL) was added, and the resulting mixture was heated at 100 °C for 16 h. After cooling to room temperature, the reaction mixture was poured into an excess of saturated aqueous sodium hydrogen carbonate solution (50 mL) and stirred for 15 min. Subsequently, the reaction mixture was extracted with dichloromethane (3×50 mL). The combined organic layers were washed with brine (50 mL), dried over sodium sulfate, and reduced in a vacuum. The crude product was purified by flash column chromatography over silica gel to afford oxadiazole compounds **TCz-Me-Ox, TCz-ArF-Ox and TCz-AlkF-Ox**.

Photophysical Characterization Procedure

Absorption measurements were taken with a Lambda 1050 spectrophotometer (Perkin Elmer). For the steady-state and transient photoluminescence measurements, an FLS980 (Edinburgh Instruments) fluorimeter using an Xe900 xenon lamp head (Edinburgh Instruments) and a 379 nm laser (PLD800D and LDH–D-C-375, Picoquant) was employed.

Theoretical Calculations

For DFT and TD-DFT calculations, Gaussian 16 Rev. C.01[29] was employed, utilizing the meta-GGA-hybrid BMK[30] functional developed by Boese and Martin in 2004, a method well-known for its efficiency in simulating TADF systems.[10,31–33] The geometry optimization (followed by the vibrational analysis) and computation of vertical excitation energies (i.e., singlets and triplets) were performed with the def2-SVP[34] basis set incorporating Grimme's D3-dispersion correction with Becke-Johnson damping (D3(BJ)).[35] To compute the singlet excited states, the Tamm-Dancoff approach (TDA-DFT)[36] was applied, while the UBMK approach was used to optimize T_1. Both vertical and adiabatic (including ZPVE) on S–T energy gaps were calculated. All calculations were performed in the gas phase. A default ultra-fine grid for numerical integrations and an energy convergence criterion of 10^{-8} Hartree were employed. The computational approach was validated and cross-referenced with experimental data, i.e., UV-vis spectra of emitters (Figure S16). Rates and reorganization energies (λ) were computed using MOMAP Version 2022 A (2.3.3).[37] Meanwhile, Spin-Orbit Coupling calculations were conducted using ADF 2020.1[38] and ORCA Version 4.2.1 [39]) software, accounting for relativistic effects. Rates were computed considering the integration time step of 0.1 fs without including Duschinsky rotation. A detailed explanation of the methodology used for the computation of radiative and non-radiative rates is provided in the supporting information. Molecular orbitals analysis was conducted using a combination of the Multiwfn analyzer (version 3.6)[40] and VMD software (version 1.9.4a48).[41] The CT data and electron-hole analysis, including the visualization of their respective contributions, were conducted using the Multiwfn analyzer.

Supporting Information Summary

Detailed synthetic methods, NMR spectra, spectroscopic data, and computational data can be found in the Supporting Information.

Authors Contributions

Céline Leonhardt: Writing – original draft, Visualization, Validation, Methodology, Investigation, Formal analysis, Data curation, Conceptualization. Anna Mauri: Writing – review & editing, Writing – original draft, Visualization, Validation, Software, Methodology, Investigation, Formal analysis, Data curation, Conceptualization. Idoia Garin: Writing – original draft, Visualization, Validation, Methodology, Investigation, Formal analysis, Data curation. Nils W. Rosemann: Writing – review & editing, Validation. Wolfgang Wenzel: Writing – review & editing, Resources, Methodology, Funding acquisition. Uli Lemmer: Writing – review & editing, Resources, Methodology, Funding acquisition. Mariana Kozlowska: Writing – review & editing, Writing – original draft, Investigation, Formal analysis, Validation, Supervision, Project administration, Methodology, Formal analysis, Conceptualization. Stefan Bräse: Writing – review & editing, Validation, Supervision, Resources, Funding acquisition, Methodology, Conceptualization.

Acknowledgements

This research has been funded by Deutsche Forschungsgemeinschaft (DFG, German Research Foundation) under Germany's

Excellence Strategy for the Excellence Cluster "3D Matter Made to Order" (Grant No. EXC-2082/1–390761711) and by the Carl Zeiss Foundation. The authors acknowledge support by the state of Baden-Württemberg through bwHPC and the DFG through grant no INST 40/575-1 FUGG (JUSTUS 2 cluster) under project bw20F004. Financed by the Ministry of Science, Research and the Arts of Baden-Württemberg as part of the sustainability financing of the projects of the Excellence Initiative II. We acknowledge support by the KIT-Publication Fund of the Karlsruhe Institute of Technology. Open Access funding enabled and organized by Projekt DEAL.

Conflict of Interests

The authors declare no conflict of interest.

Data Availability Statement

The data that support the findings of this study are available on request from the corresponding author. The data are not publicly available due to privacy or ethical restrictions.

Keywords: Thermally activated delayed fluorescence · Design strategy · Photoluminescence · Photophysical rates · Charge transfer properties · Density functional theory

[1] Z. Yang, Z. Mao, Z. Xie, Y. Zhang, S. Liu, J. Zhao, et al., *Chem. Soc. Rev.* **2017**, *46*(3), 915–1016.
[2] A. Endo, M. Ogasawara, A. Takahashi, D. Yokoyama, Y. Kato, C. Adachi, *Adv. Mater.* **2009**, *21*(47), 4802–6.
[3] X. K. Chen, D. Kim, J. L. Brédas, *Acc. Chem. Res.* **2018**, *51*(9), 2215–24.
[4] J. M. Teng, Y. F. Wang, C. F. Chen, *J. Mater. Chem. C.* **2020**, *8*(33), 11340–53.
[5] H. Uoyama, K. Goushi, K. Shizu, H. Nomura, C. Adachi, *Nature.* **2012**, *492*(7428), 234–8.
[6] C. Bizzarri, F. Hundemer, J. Busch, S. Bräse, *Polyhedron* **2018**, *140*, 51–66.
[7] M. Y. Wong, E. Zysman-Colman, *Adv. Mater.* **2017**, *29*(22), 1605444.
[8] T. T. Bui, F. Goubard, M. Ibrahim-Ouali, D. Gigmes, F. Dumur, *Beilstein J. Org. Chem.* **2018**, *14*, 282–308.
[9] D. Zhang, X. Cao, Q. Wu, M. Zhang, N. Sun, X. Zhang, et al., *J. Mater. Chem. C.* **2018**, *6*(14), 3675–82.
[10] R. Haldar, M. Jakoby, M. Kozlowska, M. Rahman Khan, H. Chen, Y. Pramudya, et al., *Chem. Eur. J.* **2020**, *26*(71), 17016–20.
[11] A. Endo, K. Sato, K. Yoshimura, T. Kai, A. Kawada, H. Miyazaki, et al., *Appl. Phys. Lett.* **2011**, *98*(8), 083302.
[12] G. Kreiza, D. Banevičius, J. Jovaišaitė, K. Maleckaitė, D. Gudeika, D. Volyniuk, et al., *J. Mater. Chem. C.* **2019**, *7*(37), 11522–31.
[13] D. Zhang, M. Cai, Y. Zhang, D. Zhang, L. Duan, *Mater. Horiz.* **2016**, *3*(2), 145–51.
[14] D. Zhang, X. Song, A. J. Gillett, B. H. Drummond, S. T. E. Jones, G. Li, et al., *Adv. Mater.* **2020**, *32*(19), 1908355.
[15] Y. Shi, H. Ma, Z. Sun, W. Zhao, G. Sun, Q. Peng, *Angew. Chem. Int. Ed.* **2022**, *61*(51), e202213463.
[16] K. Wang, C. Zheng, W. Liu, K. Liang, Y. Shi, S. Tao, et al., *Adv. Mater.* **2017**, *29*(47), 1701476.
[17] H.-Z. Li, D. Zhang, F.-M. Xie, X. Y. Zeng, Y. Q. Li, H.-X., Wei, et al. *Dyes Pigm.* **2021**, *188*, 109210.
[18] R. Huisgen, J. Sauer, H. J. Sturm, J. H. Markgraf, *Chem. Ber.* **1960**, *93*(9):2106–24.
[19] Y. Wada, H. Nakagawa, S. Matsumoto, Y. Wakisaka, H. Kaji, *Nat. Photonics.* **2020**, *14*(10), 643–9.
[20] J. U. Kim, I. S. Park, C. Y. Chan, M. Tanaka, Y. Tsuchiya, H. Nakanotani, et al., *Nat. Commun.* **2020**, *11*(1), 1765.
[21] J. L. Bredas, *Mater. Horiz.* **2014**, *1*(1), 17–9.
[22] F. B. Dias, T. J. Penfold, A. P. Monkman, *Methods Appl. Fluoresc.* **2017**, *5*(1), 012001.
[23] S. Wu, L. A. Galán, M. Roux, F. Riobé, B. Le Guennic, Y. Guyot, et al., *Inorg. Chem.* **2021**, *60*(21), 16194–203.
[24] N. Haase, A. Danos, C. Pflumm, P. Stachelek, W. Brütting, A. P. Monkman, *Mater. Horiz.* **2021**, *8*(6), 1805–15.
[25] C. Guerra, L. Ayarde-Henríquez, Y. A. Rodríguez-Núñez, A. Ensuncho, E. Chamorro, *ChemPhysChem.* **2023**, *24*(11), e202200867.
[26] T. H. Kwon, S. O. Jeon, M. Numata, H. Lee, Y. S. Chung, J. S. Kim, et al., *Nanomaterials* **2019**, *9*(12), 1735.
[27] D. Hall, J. C. Sancho-García, A. Pershin, G. Ricci, D. Beljonne, E. Zysman-Colman, et al., *J. Chem. Theory Comput.* **2022**, *18*(8), 4903–18.
[28] R. Gómez-Bombarelli, J. Aguilera-Iparraguirre, T. D. Hirzel, D. Duvenaud, D. Maclaurin, M. A. Blood-Forsythe, et al., *Nat. Mater.* **2016**, *15*(10), 1120–7.
[29] M. J. Frisch, G. W. Trucks, H. B. Schlegel, G. E. Scuseria, M. A. Robb, J. R. Cheeseman et al. Gaussian 16 Gaussian, Inc, Wallingford, CT **2016**.
[30] A. D. Boese, J. M. L. Martin, *J. Chem. Phys.* **2004**, *121*(8), 3405–16.
[31] S. Feng, X. Guo, J. Zhang, *Spectrochim. Acta A Mol. Biomol. Spectrosc.* **2020** *226*, 117564.
[32] K. Shizu, Y. Ren, H. Kaji, *J. Phys. Chem. A.* **2023**, *127*(2), 439–49.
[33] Q. Zhu, X. Guo, J. Zhang, *J Comput Chem.* **2019**, *40*(16), 1578–85.
[34] A. Schäfer, H. Horn, R. Ahlrichs, *J. Chem. Phys.* **1992**, *97*(4), 2571–7.
[35] S. Grimme, S. Ehrlich, L. Goerigk, *J. Comput. Chem.* **2011**, *32*(7), 1456–65.
[36] S. Hirata, M. Head-Gordon, *Chem. Phys. Lett.* **1999**, *314*(3–4), 291–9.
[37] Y. Niu, W. Li, Q. Peng, H. Geng, Y. Yi, L. Wang, et al., *Mol. Phys.* **2018**, *116*(7–8), 1078–90.
[38] G. te Velde, F. M. Bickelhaupt, E. J. Baerends, C. Fonseca Guerra, S. J. J. van Gisbergen, J. G. Snijders, et al. *J. Comput. Chem.* **2001**, *22*(9), 931–67.
[39] F. Neese, *WIREs Comput. Mol. Sci.* **2012**, *2*(1), 73–8.
[40] T. Lu, F. Chen, *J. Comput. Chem.* **2012**, *33*(5), 580–92.
[41] W. Humphrey, A. Dalke, K. Schulten, *J. Mol. Graph.* **1996**, *14*, 33–8.

Manuscript received: April 29, 2024
Accepted manuscript online: June 27, 2024
Version of record online: September 3, 2024